

A Real Space Description of Magnetic Field Induced Melting in the Charge Ordered Manganites: I. The Clean Limit

Anamitra Mukherjee¹ and Pinaki Majumdar²

¹*Department of Physics and Astronomy, University of British Columbia, Vancouver, BC, Canada, V6T 1Z1 and*

²*Harish-Chandra Research Institute, Chhatnag Road, Jhusi, Allahabad 211019, India*

(Dated: February 12, 2022)

We study the melting of charge order in the half doped manganites using a model that incorporates double exchange, antiferromagnetic superexchange, and Jahn-Teller coupling between electrons and phonons. We primarily use a real space Monte Carlo technique to study the phase diagram in terms of applied field (h) and temperature (T), exploring the melting of charge order with increasing h and its recovery on decreasing h . We observe hysteresis in this response, and discover that the ‘field melted’ high conductance state can be spatially inhomogeneous even without extrinsic disorder. The hysteretic response plays out in the background of field driven equilibrium phase separation. Our results, exploring h , T , and the electronic parameter space, are backed up by analysis of simpler limiting cases and a Landau framework for the field response. This paper focuses on our results in the ‘clean’ systems, a companion paper studies the effect of cation disorder on the melting phenomena.

I. INTRODUCTION

Study of correlated materials such as the cuprates, the pnictides and the manganites is motivated as much by fascinating phenomena as by the opportunity to understand many body physics. In this respect manganites provide a perfect example, hosting phenomena such as colossal magnetoresistance (CMR)^{1,2} and multiferroic behavior³ on the one hand, while offering a window on how strongly coupled degrees of freedom organize and respond to external stimuli^{4–7}.

This has given great impetus to experimental and theoretical research on phenomenology and microscopic understanding of the manganites. Experimental work has probed in detail, the doping and temperature dependence of phases and transport properties^{4,8} in the past. More recent focus has been towards controlling phases and transport properties using a variety of schemes such as substrate induced strain on thin films^{9–14}, heterojunctioning different manganites^{15–18} and using electric fields^{19,20}. Finally the field of possible device applications has been very active^{21–24}.

Calculations based on model Hamiltonians using a variety of techniques has culminated in the understanding of the microscopic basis for CMR^{5,25,26}. Interplay of disorder, strain and impurity physics in the background on phase competition has also been extensively studied, these are discussed later in the text.

There has also been growing interest in investigating impact of time dependent probes such as pump-probe experiments and optical excitation^{27–31} on the manganites. These and similar studies with magnetic and thermal field cycling^{32–38} have made understanding of nonequilibrium properties of the manganites very pertinent. At present, however, the theoretical study of nonequilibrium response in the manganites has received little attention. The goal of the present paper and its companion is to address some of these issues. For this we study the effects of magnetic field sweeps on spin charge orbital ordered phases in the half doped manganites. To set the stage, we

briefly summarize the basic properties of the manganites.

Among the plethora of phases that the manganites exhibit^{4,8}, of particular interest are the ferromagnetic metal (FM-M) and the antiferromagnetic charge ordered insulating (AF-CO-I) states. The ferromagnetic metal usually shows up in manganites with large bandwidth (BW), *i.e.*, large mean cation radius, r_A , for hole doping $x \sim 0.2 - 0.5$, while the AF-CO-I state is observed in low bandwidth materials at commensurate doping, $x \sim 0.5$. This ‘half doped’ state is especially interesting since it allows systematic study of phase competition and the role of disorder. The $x = 0.5$ state has been extensively probed experimentally^{32–34,39–48} and also analyzed theoretically^{5,49–52}.

It is known that low bandwidth materials with CE magnetic order, checkerboard charge order (CO), and concomitant orbital order (OO), are insulating. We will call this state CE-CO-I. The large BW materials have a FM-M ground state. At intermediate BW some materials have ‘A type’ magnetic order. Application of a magnetic field can melt the charge order and convert the CE-CO-I to a ferromagnetic metal. The melting transition appears to be abrupt and is accompanied by hysteresis in response to field sweep^{4,8,32,33}.

Crudely, the CO state in manganites ‘melts’ in response to a magnetic field because the field favors FM order to CE order, and the CO stability depends on the CE order. Some aspects of the melting problem are well studied. (i) The thermodynamic melting field h_c (which is bracketed by the actual switching fields, h_c^\pm , discussed later) is small. The associated energy scale $g\mu_B h_c \ll k_B T_{CO}$, where T_{CO} is the zero field melting temperature (g is the gyromagnetic ratio and μ_B the Bohr magneton). The smallness of h_c is attributed to the small energy difference between the CE-CO-I and FM-M states. (ii) The field induced transition is seen to be first order and is accompanied by hysteresis since there are competing metastable minima, particularly for materials close to the CE-CO-I - FM-M phase boundary. (iii) The field induced FM-M is believed to be homogeneous, and is

so assumed in theoretical studies. These general observations set important benchmarks for any detailed theory, but some key issues remained unresolved.

(i) *The nature of the finite field state:* Recent experiments^{34,44–48} have demonstrated that the melted state is actually inhomogeneous. We show that at half doping, for materials with weak charge-orbital order, *an applied field induces phase separation* and the ‘melted’ state is at best a percolative metal.

(ii) *The field driven equilibrium transition:* We contend that the *equilibrium transition* should be continuous. Above a threshold, an applied field actually leads to phase separation into AF-CO-I and FM-M regions, with gradual increase of the FM-M fraction with increasing field. The experimentally (and computationally) observed abrupt field driven transition between the CE-CO-I and the notional ‘FM-M’ states is a non-equilibrium effect due to neighboring metastable states.

(iii) *Switching fields and limits of metastability:* While the thermodynamic critical field can be estimated from energy balance, the upper and lower critical fields that are actually measured define limits of metastability, and have not been explored theoretically till now. We calculate these, and compare to experimental scales.

(iv) *The effect of disorder on field melting:* One expects h_c to increase with reducing bandwidth, since the CO is better stabilized. This indeed happens for lanthanides (Ln) of the form³⁹ $\text{Ln}_{1/2}\text{Ca}_{1/2}\text{MnO}_3$. For members of the $\text{Ln}_{1/2}\text{Sr}_{1/2}\text{MnO}_3$ family^{40–42}, with very similar bandwidths, h_c increases initially with decreasing BW but takes a *downturn* beyond a critical BW and then drops to zero, in sharp contrast to the ‘divergence’ of h_c seen in the Ca family. We explain this in terms of the reduced stiffness of the CO state in the presence of disorder⁵³.

In our earlier short paper⁵⁴ we had touched upon some of the issues above. This paper provides a thorough exploration of the parameter space of the underlying model, focusing on the interplay of equilibrium phase separation and the sweep rate induced non-equilibrium effects.

We have mapped out the $h - T$ phase diagrams capturing both hysteresis and re-entrant features as seen in experiments. In addition to thermodynamic indicators we have characterized the system at low temperature through direct spatial snapshots and by measuring the volume fraction of the CO-I and the FM-M. Our results allow us to provide comprehensive answers to issues (i)-(iv) listed earlier. Further, by putting our results within a Landau-like energy landscape, we have provided a broad framework for organizing the materials systematics.

The paper is organized as follows. In section II we summarize the key experimental results, and follow it in section III with a discussion of earlier theoretical work on field melting. In section IV we define our model and describe the method for solving it. Section V discusses the zero field reference state. Section VI is the heart of the paper and discusses the results at finite field. In sections VII-VIII, we analyze these results in terms of alternate simpler calculations, provide a Landau framework. We

conclude in section IX.

II. EXPERIMENTAL RESULTS

Ca	Sr	Ba							
1.34	1.44	1.61							
La	Pr	Nd	Sm	Eu	Gd	Tb	Ho	Y	
1.36	1.29	1.27	1.24	1.23	1.21	1.20	1.18	1.18	

TABLE I. Ionic radii (in Angstroms) for various AE^{2+} and RE^{3+} ions in the perovskite manganites⁸.

Experiments on the field response of the CO state have probed hysteresis, the bandwidth dependence of the melting fields and the effect of disorder through transport measurements and spatial imaging of magnetic correlations in the lattice. We briefly review the important results here.

The key material systematics are embodied in the magnetic field-temperature ($h - T$) phase diagrams for different materials, shown in Fig.1. These are based on the investigations of two lanthanide families, the Ca series³⁹, $\text{Ln}_{0.5}\text{Ca}_{0.5}\text{MnO}_3$, and the Sr series^{40–42}, $\text{Ln}_{0.5}\text{Sr}_{0.5}\text{MnO}_3$. The bandwidth is varied by making materials with Ln atoms with progressively smaller radius (see Table. 1). In Fig.1, r_A reduces progressively from $\text{Pr}_{0.5}\text{Sr}_{0.5}\text{MnO}_3$ (PSMO) to $\text{Sm}_{0.5}\text{Ca}_{0.5}\text{MnO}_3$ (SCMO). The phase diagrams were constructed by sweeping up and down in magnetic fields, at fixed temperature, on samples that had been initially zero field cooled. The melting field in the upward sweep (h_c^+) differs the most from the ‘recovery’ field (h_c^-) in the downward sweep when $T \rightarrow 0$. This difference narrows and vanishes as $T \rightarrow T_{CO}$.

h_c^- shows a ‘re-entrant’ feature in the intermediate BW materials, *decreasing with reducing temperature*. Reducing BW (or reducing r_A) progressively increases the stability of the CO state, with SCMO having the largest h_c^\pm and T_{CO} .

The half-doped materials are also, inevitably, disordered. The Ln and alkaline earth atoms usually have different ionic radius, and an ‘alloy’, with these randomly located lead to variations in the local electronic parameters. For example, it leads to random changes in the Mn-O-Mn bond angles, θ say, modulating the local hopping, $\propto \cos^2(\theta)$. The other effect is ‘charge scattering’ since the Ln and alkaline earth have different valence. Typically the extent of structural disorder is quantified by the variance σ_A of the ionic radii of the A site ions and its effect has been studied in the Ca, Sr, and Ba families^{55–57}. Near $x = 0.5$, the variance in the Ca family is $\sigma_A \sim 10^{-3}\text{\AA}^2$, for the Sr family greater mismatch leads to $\sigma_A \sim 10^{-2}\text{\AA}^2$. We will consider the Ca family to represent the a ‘clean’ manganite, the Sr family is typical

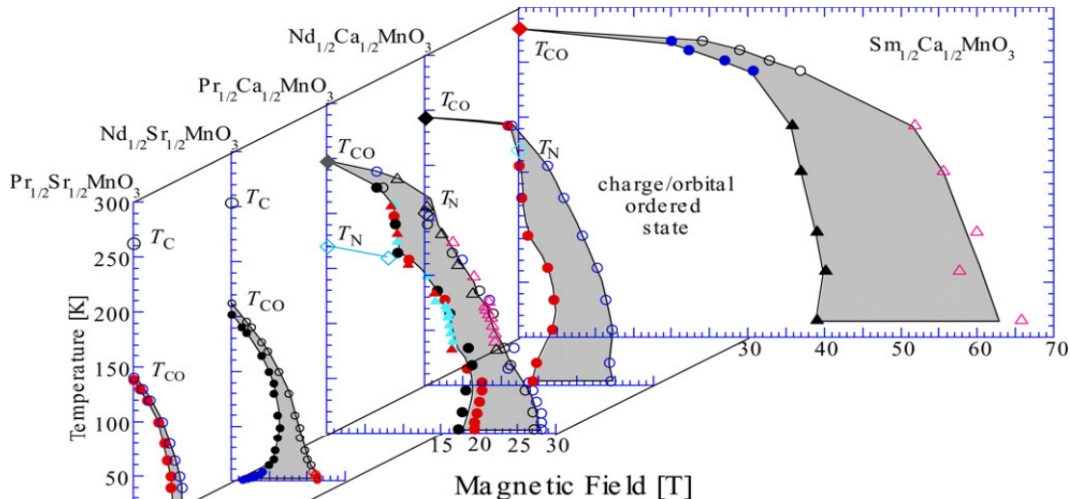


FIG. 1. Colour online: The h - T phase diagram of various $\text{RE}_{1/2}\text{AE}_{1/2}\text{MnO}_3$ compounds⁸. The materials involve a systematic decrease in r_A from $\text{Pr}_{0.5}\text{Sr}_{0.5}\text{MnO}_3$ (PSMO) to $\text{Sm}_{0.5}\text{Ca}_{0.5}\text{MnO}_3$ (SCMO). The critical CO melting temperatures increase with decreasing r_A . The associated hysteresis opens a window of metastability at low T , which tapers with increase in temperature and vanishes at T_{CO} . The Ca family has low disorder and shows re-entrant behavior in h_c^- , which vanishes at very low bandwidths ($\text{Sm}_{0.5}\text{Ca}_{0.5}\text{MnO}_3$). Further, in the Ca family, the decrease in r_A , also makes the CO state more robust, with SCMO having the largest melting fields. The Sr family has larger disorder (see text) with $\text{Pr}_{0.5}\text{Sr}_{0.5}\text{MnO}_3$ having larger r_A than $\text{Nd}_{0.5}\text{Sr}_{0.5}\text{MnO}_3$ (NSMO). While NSMO shows marked hysteresis, PSMO is rather benign.

of moderate disorder, while the Ba family involves strong disorder.

The impact of disorder on the zero field $x = 0.5$ state has been beautifully demonstrated⁵⁸ by careful preparation of 'non-disordered' samples. This experiment focused on the transition temperatures as a function of disorder. More recent experiments have begun to explore the spatial nature of the melting process^{34,44} and the role of disorder⁴⁵⁻⁴⁷ in it. The following broad picture has emerged from these studies: (a) The melting fields increase with decreasing r_A in the Ca family but they are *suppressed* on decreasing r_A in the Sr family. For the Ba family, long range CO is absent even at zero field due to the large structural disorder. (b) Spatial probes suggest, for example, that in NSMO⁴⁴ the low T finite field state is inhomogeneous, with 'poor FM' domains coexisting with perfect FM regions. Similar results were reported in $\text{La}_{\frac{5}{8}-y}\text{Pr}_y\text{Ca}_{\frac{3}{8}}\text{MnO}_3$ where CO-I regions are shown to coexist with FM-M regions. (c) Some experiments^{47,48} in LCMO, PCMO, PSMO and NSMO at $x = 0.5$ indicate coexistence, at low T , of competing AF-I and FM-M phases with h - T protocol dependent tunable volume fractions. Additionally, short temporal magnetic field pulses on (LCMO at $x = 0.5$) has been reported to cause a switching effects in the volume fraction of charge order, precisely anticorrelated to the magnetic pulse³⁷.

III. STATUS OF THEORY

Theory of manganites is fairly evolved. Manganites have been modeled with varying degree of realism with a number of techniques including dynamical mean field theory (DMFT)²⁵, density functional theory+DMFT⁵⁹, variational approaches^{50,51}, and exact diagonalization coupled with Classical Monte Carlo^{5,26}. These have been used to study low temperature phases⁶⁰⁻⁶⁷, doping and disorder effects^{54,68-70}, dynamical properties⁷¹, transport^{68,72,73} and the CMR response⁷⁴⁻⁷⁶. Beyond bulk manganites, manganite heterojunctions^{77,78}, strain effects on thin films^{72,79,80}, are being investigated. Further, the coupling between spin, charge and orbitals has been studied to understand multiferroic behavior⁸¹⁻⁸⁶.

However the area of nonequilibrium response to external perturbations has however received little attention. Given current experiments probing photo excitation of correlated phases, phase fractions dependence on path taken in temperature-magnetic field variation protocols and field sweeps effects, clear understanding of non equilibrium physics is very relevant. Before we turn to our results, below we briefly survey the limited literature existing in this area.

More specifically at half doping, the metal insulator transitions with changing bandwidth with isovalent A site substitution has lead to remarkable agreement between theory and experiment. The stability of the small BW CE-CO-I phase and the nature of charge order extensively discussed. Indeed there has been considerable debate

between Zener polaron type charge order, involving both Mn and oxygen on the one hand and charge disproportionation involving only Mn atoms on the other.

There have been some attempts at a theory of field induced melting in CO manganites^{49–52}.

(i) The earliest attempt⁴⁹ involved the mean field study of a one band model with on-site and nearest neighbor Hubbard interaction in addition to double exchange. On application of a magnetic field, the zero field AF-CO-I state was shown to melt to a FM-M through a first order transition. The result shows that a CO state could be destabilized by a magnetic field which couples only to the magnetic sector.

(ii) A variational study was done for a more realistic model⁵⁰ incorporating, Jahn-Teller interaction and a class of charge ordered/metallic states with variety of magnetic order (FM, G-AF, CE-AF). This established that decrease in BW resulted in an increase in magnetic melting (energy crossing) fields.

(iii) Finally, a two orbital model was studied, with a large family of variational states in a recent work⁵¹. This established that the smallness of the (thermodynamic) melting field is due to the closeness in energy of the CE-CO-I and the FM-M phases. For a range of electron-phonon coupling they discovered that a CE-CO state with ‘defects’ appears to be lower energy than a pure CE-CO or FM-M when $h \neq 0$. We believe that the result hints at a field induced inhomogeneous state but the authors did not pursue the issue further.

These experimental and theoretical results set the stage for our attempt at understanding the unresolved questions mentioned in the introduction. In particular we (i) study the spatial character of the charge and spin state under magnetic fields, (ii) examine the ‘order’ of the field melting transition, (iii) map out the dependence of the switching fields h_c^\pm on bandwidth and sweep rate, and (iv) explore the impact of disorder on the melting process.

IV. MODEL AND METHOD

A. Model

For studying the non disordered problem, we consider a two band model for e_g electrons, Hund’s coupled to t_{2g} derived core spins, in a two dimensional square (2D) lattice. The electrons are also coupled to Jahn-Teller phonons, while the core spins have an AF superexchange coupling between them. These ingredients are all necessary to obtain a CE-CO-I phase.

$$H = - \sum_{\langle ij \rangle \sigma} \sum_{\alpha\beta} t_{\alpha\beta}^{ij} c_{i\alpha\sigma}^\dagger c_{j\beta\sigma} - J_H \sum_i \mathbf{S}_i \cdot \boldsymbol{\sigma}_i + J \sum_{\langle ij \rangle} \mathbf{S}_i \cdot \mathbf{S}_j - \lambda \sum_i \mathbf{Q}_i \cdot \boldsymbol{\tau}_i + \frac{K}{2} \sum_i \mathbf{Q}_i^2 - \mu N - h \sum_i S_{iz} \quad (1)$$

Here, c and c^\dagger are annihilation and creation operators for e_g electrons and α, β are the two Mn- e_g orbitals $d_{x^2-y^2}$ and $d_{3z^2-r^2}$, labeled (a) and (b) in what follows. $t_{\alpha\beta}^{ij}$ are hopping amplitudes between nearest-neighbor sites with the symmetry dictated form: $t_{aa}^x = t_{aa}^y \equiv t$, $t_{bb}^x = t_{bb}^y \equiv t/3$, $t_{ab}^x = t_{ba}^x \equiv -t/\sqrt{3}$, $t_{ab}^y = t_{ba}^y \equiv t/\sqrt{3}$, where x and y are spatial directions. The e_g electron spin is $\sigma_i^\mu = \sum_{\sigma\sigma'} c_{i\alpha\sigma}^\dagger \Gamma_{\sigma\sigma'}^\mu c_{i\alpha\sigma'}$, where the Γ ’s are Pauli matrices. It is coupled to the t_{2g} spin \mathbf{S}_i via the Hund’s coupling J_H . λ is the coupling between the JT distortion $\mathbf{Q}_i = (Q_{ix}, Q_{iz})$ and the orbital pseudospin $\boldsymbol{\tau}_i^\mu = \sum_{\sigma} c_{i\alpha\sigma}^\dagger \Gamma_{\alpha\beta}^\mu c_{i\beta\sigma}$, and K is the lattice stiffness, and h the magnetic field. We assume it to be in the z direction and coupled only to \mathbf{S}_i . We set $t = 1$, $K = 1$, and treat the \mathbf{Q}_i and \mathbf{S}_i as classical variables. The magnitude ($S=3/2$) of the core spin is absorbed in the coupling constants. The chemical potential μ is adjusted so that the electron density remains $n = 1/2$ which is also $x = 1 - n = 1/2$.

B. Parameter space

In the manganites $J_H/t \gg 14$ ⁵. We choose λ/t and J/t such that the ground state is CE-CO-I at $h = 0$, but close to a FM-M phase, in accordance to the well established closeness of the energies of these phases in the manganites⁵. Changing λ is equivalent to change in (inverse) BW. BW variation in materials (by changing r_A) in mimicked by suitably varying λ . In reality J also changes with BW variation, but for simplicity, we assume it to be independent and explore only a couple of J values, $J = 0.10, 0.12$. The choice is justified later in the text.

C. Method

We use a variant of the usual real space exact diagonalization (ED) based Monte Carlo (MC) method⁵. In the usual ED+MC the computation cost scales as N^4 , N being the size of the system. Within our method, the so called ‘traveling cluster approximation’ (TCA), the computational cost for the same system is $\sim NN_C^3$, where N_C is the *fixed* cluster size, and is *linear* in N as opposed to N^4 . Since the TCA approach is well established, to avoid repetition, we refer to existing literature⁸⁷ for details. Using this technique we have accessed sizes up to 40^2 as opposed to the limit of $\sim 10^2$ within ED+MC.

The present work is in the spirit of several earlier calculations^{88–91}, where Monte Carlo technique has been employed to explore the non-equilibrium effects like hysteresis etc., around a phase transition.

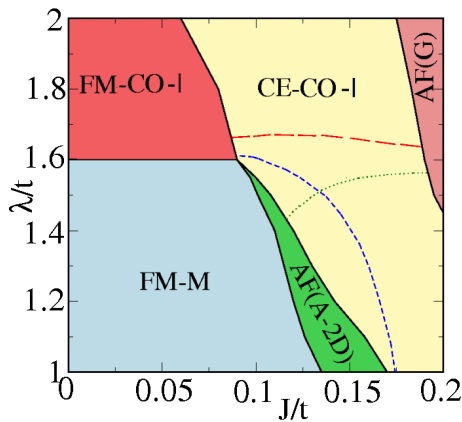


FIG. 2. Colour online: The $\lambda - J$ phase diagram at $T/t = 0.01$. The various phases are indicated in the colored regions separated by solid lines. See text for details. For field induced melting at reasonable h , we need to explore the vicinity of $\lambda/t \sim 1.6$, $J/t \sim 0.10$. The dashed/dotted lines, demarcate various parameter regimes in the CE-CO-I phase in terms of their response to a magnetic field. For large λ (above the big-dashed line), the CO state does not melt on applying a field. Between the big dashed line and the finely dashed line the CO melts on field application and recovers when the field is reduced. Between the finely dashed line and the AF-2D phase boundary the field melted CO does not recover on field removal. Further, the region below the dotted line, the CE-CO-I state melts to a homogeneous FM-M, while that above it melts to an inhomogeneous state. The zero field phases are discussed in section V and the magnetic response will be discussed in section VI.

D. Physical quantities

In order to study the evolution with applied magnetic field, we track various correlation functions involving the charge, spin, and lattice degrees of freedom. These include the following:

1. The distribution of lattice distortions, $P(Q) = \langle \sum_i \delta(Q - Q_i) \rangle$, where $Q_i = |\mathbf{Q}_i|$ is the magnitude of the Jahn-Teller distortion at site i . Angular brackets represent thermal average.
2. The structure factor for lattice distortions, $D_Q(\mathbf{q}) = \sum_{ij} \langle \mathbf{Q}_i \cdot \mathbf{Q}_j \rangle e^{i\mathbf{q} \cdot (\mathbf{r}_i - \mathbf{r}_j)}$. This is also a measure of the charge-charge correlation since the local charge density, n_i , approximately follows Q_i .
3. The magnetic structure factor, $S(\mathbf{q}) = \frac{1}{N^2} \sum_{ij} \langle \mathbf{S}_i \cdot \mathbf{S}_j \rangle e^{i\mathbf{q} \cdot (\mathbf{r}_i - \mathbf{r}_j)}$.
4. The volume fraction of charge order, V_{CO} , obtained by analyzing the real space density distribution. A site with $n_i > 0.5$, surrounded by four sites with $n_i < 0.5$ is part of a CO pattern. Counting such sites allows us to compute the volume of charge ordered regions *even if long range order is lost*. This

is particularly useful in an inhomogeneous situation.

5. The electronic density of states (DOS) is computed as $N(\omega) = \langle \frac{1}{N} \sum_n \delta(\omega - \epsilon_n) \rangle$, where ϵ_n are the electronic eigenvalues in a given equilibrium $\{Q, S\}$ configuration.
6. The (low frequency) conductivity σ_{dc} , is computed from the matrix elements of the current operator, as described elsewhere⁹².

V. RESULTS AT ZERO FIELD

We start with the $\lambda - J$ phase diagram at zero field. It helps identify phases that compete with the CE-CO-I state. This allows us to fix parameter regime for our finite field result. Additionally this phase diagram will be later used to classify different zero field CE-CO-I regimes that respond differently to magnetic field sweeps.

Fig.2 shows the $\lambda - J$ phase diagram⁹³ where the various phases obtained are indicated. The solid lines are first order phase boundaries and are determined by annealing from high to low temperature at zero field. The evolution with increasing J/t for $\lambda/t < 1.6$ consists of going from FM-M to A-2D to CE-CO-I to G-AF. The A-2D is a metallic phase with $(\pi, 0)$ or $(0, \pi)$ magnetic order, that lives in narrow region below $\lambda/t \sim 1.6$. For $\lambda/t < 1.6$ the CE-CO-I requires the 'CE' pattern to reduce the BW where upon the electron-phonon (e-p) term becomes dominant causing the CO. However at large $\lambda/t (> 1.6)$ we find that the (e-p) term is strong enough to stabilize the CO state even in a FM state as is seen in the top left part of Fig.2. Increasing J/t for $\lambda/t > 1.6$ simply evolves the magnetic sector almost independent of the CO state, from FM to CE to G-AF. This implies that for this regime (of small BW), the magnetic field on the CE-CO-I would cause a transition only to a FM-CO-I and would not melt the CO state. This small BW region is marked by the large dashed (red) line.

We can now justify choice of $J/t \sim 0.1$ values as follows. If we are in a parameter regime where the FM-M and CE-CO-I phases are very close in energy, $\lambda/t \sim 1.6$ and $J/t \sim 0.10$, we can drive a CE-CO-I to FM-M transition by applying a small magnetic field. In the present work we use $J/t = 0.10$ and $J/t = 0.12$. $J/t = 0.10$ allows closer agreement of temperature and magnetic scales to experiments as was shown in our earlier work⁹³. However, $J/t = 0.1$ does not allow much room to explore the λ/t dependence. The available λ/t window ($\Delta\lambda$) is ~ 0.1 . At the lower end one hits the A-2D phase and at the upper end is the large dashed red line, above which the CO-state cannot be field melted. For exploring the BW dependence in more detail we choose $J/t = 0.12$ allowing a window $\Delta\lambda \approx 0.2$, while we still remain in the correct ballpark of the experimental transition scales.

The dashed/dotted lines, obtained by magnetic field sweeps at fixed low temperature, indicate the boundaries

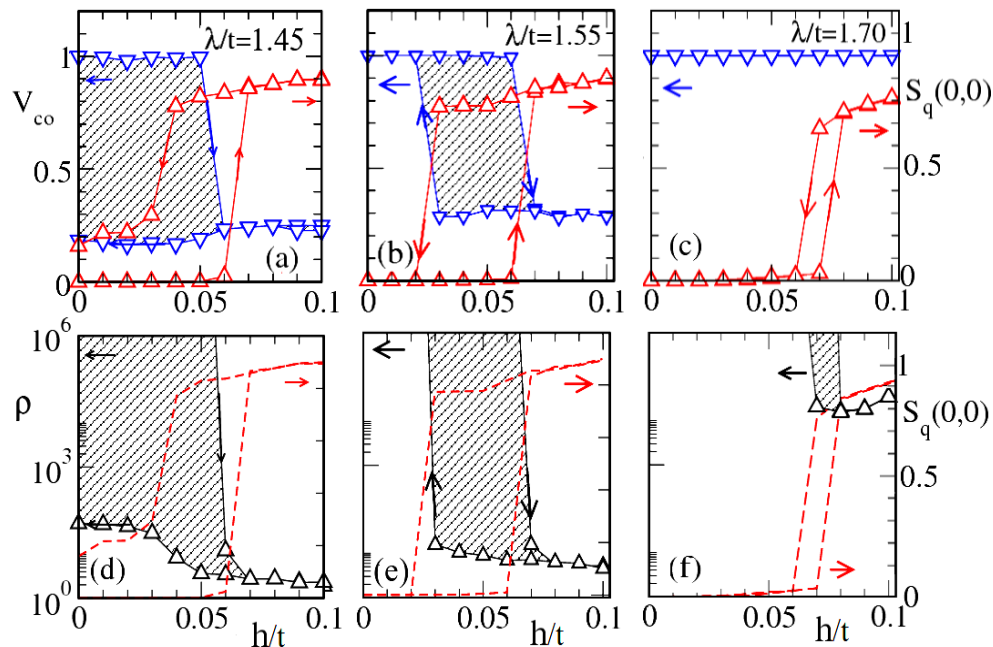


FIG. 3. Colour online: Distinct response to field cycling as a function of λ . Top panel, (a) to (c), shows V_{CO} and $S_q(0,0)$ and bottom panel, (d) to (f), shows the corresponding resistivity as a function of the applied magnetic field at increasing λ values. The λ values are indicated, $J/t = 0.12$ and $T=0.02$. In (a) and (b) increasing the field causes V_{CO} to switch at h_c^+ . This is accompanied by a CE to FM transition as $S_q(0,0)$ shows. There is corresponding drop in ρ as well. In the reverse part of the sweep, V_{CO} switches back to '1' at h_c^+ in (b) but does not recover in (a). In (c) $S_q(0,0)$ switches between the CE and the FM independent of V_{CO} which remains unresponsive to the field cycling. The FM structure factor is repeated as dashed lines in the lower panels to show the correspondence with resistance switching.

of the regions showing qualitatively different response to field sweep. These are discussed in the section VI where we study the effects of a finite fields and field sweeps on the CE-CO-I phase.

VI. RESULTS AT FINITE FIELD

We consider low T magnetic field sweeps to begin with. For understanding the magnetic field effects we track the various indicators described in Sec.IV.D, by first cooling the system at $h/t = 0$ and then cycling the magnetic field. In subsection.A we provide a systematic study of the evolution of the field response with λ and in subsection.B we present our $h - T$ phase diagrams and show real space data on inhomogeneous melting.

A. Result of a typical field sweep

Fig.3 illustrates the field response for three λ, J combinations, with λ increasing from left to right. We show the CO volume fraction (V_{CO}) in blue and the ferromagnetic structure factor $S_q(0,0)$, in red, in the top panels. The corresponding resistivity $\rho(h, T)$, in black, is shown in the bottom panels. The magnetic field value (while increasing the field) that causes a switching of the CO vol-

ume fraction from unity to low values, is denoted by h_c^+ . Similarly the value of the magnetic field (when sweeping back to zero) that causes the CO volume fraction to switch back to unity, is defined as h_c^- .

Let us consider the broad differences in field response with changing λ . (i) At $\lambda/t = 1.70$, panel 3.(c), the V_{CO} is completely unresponsive to field change, while the FM structure factor grows and then shows a hysteretic decrease as expected for antiferromagnetic (CE) to FM transition. (ii) At $\lambda/t = 1.55$ the CO 'melts' in response to increasing h , but only partially, with a residual $V_{CO} \sim 0.3$. Here the magnetic transitions occur concurrently.

The lower panels, Fig.3(e)-(f) show that ρ remains very large at all h for $\lambda/t = 1.70$, while there is a distinct 'switching' for $\lambda/t = 1.55$. This state with a finite V_{CO} and but 'low' resistivity at $\lambda/t = 1.55$ is likely to be a percolative metal, with CO regions dispersed in a FM-M background. This physics is discussed later.

For $\lambda/t = 1.45$, in Fig.3(a), we again find that the high field ($h > h_c^+$) state V_{CO} is finite, but, remarkably, the CO state is *not recovered* when the field is reduced to zero. For even lower $\lambda/t \sim 1.4$ (not shown) we find a homogeneous FM-M melted state at large fields.

To summarize, we find that depending on response to applied fields as seen in Fig.3, the zero field CE-CO-I region in Fig.2, can be divided into distinct regions. These are demarcated by dashed and dotted lines in the

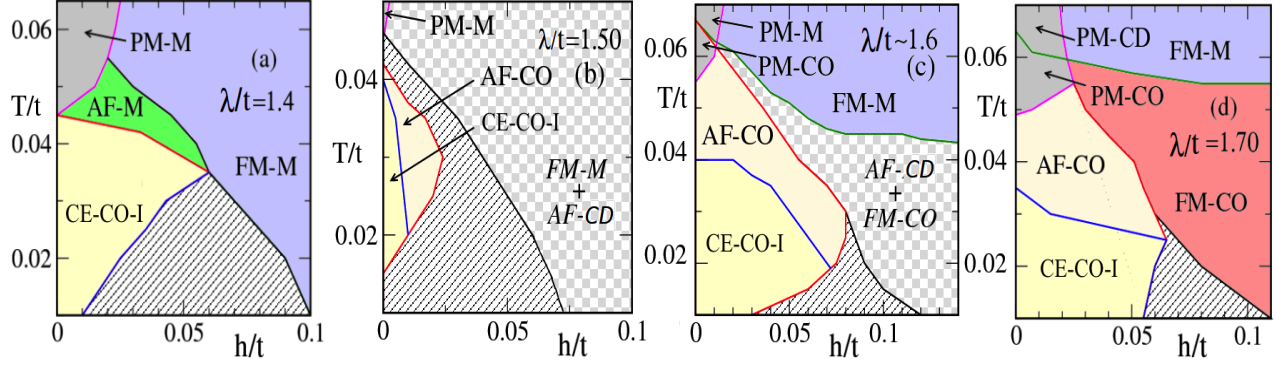


FIG. 4. Colour online: The $h - T$ phase diagrams obtained with increasing λ values from (a) to (d). At any temperature, the shaded regions imply hysteresis, light checkerboard regions imply phase separation and colored areas indicate equilibrium phases. The composition of the PS states are demarcated in italics. The gradual shift of the hysteresis window towards higher fields is expected as the CO correlations grow stronger with λ . For $\lambda/t = 1.4$ and $\lambda/t = 1.7$, which are representative of low and high λ regimes respectively, the field melted state (beyond h_c^+) is uniform. For the intermediate λ points in (b) and (c), the state beyond h_c^+ is phase separated. Note that the CO is not recovered for in (b) when the field is swept back to zero at $T/t < 0.02$. The various phases in the four panels are discussed in the text.

CE-CO-I region in Fig.2.

(i) *Melting vs non-melting*: As discussed in section V and as seen in Fig.3(c), for $\lambda/t \gtrsim 1.6$ we find the CO is independent of the CE order. Thus a magnetic field enough to induce a CE to FM transition, would simply push the system in a FM-CO-I phase. For lower λ , the CO can be melted by a magnetic field. The red (long dashed) line is the boundary.

(ii) *Homogeneous -vs- inhomogeneous melting*: Even when the CO state responds to a magnetic field, and the long range CO is destroyed, it need not result in a homogeneous FM state. As seen from the residual V_{CO} for $\lambda/t = 1.55$ beyond $h/t = 0.07$, there could be phase separation, with a surviving CO component. Overall, between the large dashed (red) line and the dotted (green) line in Fig.2, the field induced state is inhomogeneous, while below it, the state is a homogeneous FM-M.

(iii) *Recovery vs non-recovery*: The finely dashed (blue) line separates regions with different kinds of hysteretic response. Below the red large dashed line, the CO is recovered in a field sweep if it is above the blue fine-dashed line. Below this line the CO state is not recovered.

The issues of metastability in the field response and the equilibrium phase separation beyond the upper critical field (h_c^+) will be addressed in the next section.

B. The $h - T$ phase diagrams

In this subsection we discuss the thermal evolution of the low T phases by constructing $h - T$ phase diagrams. Fig.4 shows the $h - T$ phase diagrams obtained at $J/t = 0.12$ and λ values indicated, increasing from left

to right.

Thermal evolution at low fields: At low $\lambda/t \sim 1.40$ (below the green dotted line in Fig.2), with increase in temperature, the loss of the CE pattern drives the system to an AF-metallic state, with no residual CO correlations. This AF state with $S_q = (\pi, 0)$ and $S_q = (0, \pi)$ reflections is a precursor to the low temperature CE phase. This finally leads to a PM-M at higher temperatures, signifying that the electron-phonon coupling is too weak to cause an insulating PM state. The hysteresis window expectedly shrinks with increasing temperature. For $\lambda/t \geq 1.5$ the CO correlations survive at progressively higher temperatures although the long range order is suppressed. These CO regions overlap with the AF regions to form a AF-CO phase, which at higher temperatures give way to paramagnetic (PM) metal for $\lambda = 1.5$ and PM-CO at larger λ . Raising the temperature further makes the PM-CO go into PM-M or a charge disorder insulating PM depending on λ . The details of these phases will be reported elsewhere.

Thermal evolution at large fields: Let us contrast the low field evolution with that at large finite fields ($h > h_c^+$). Both for small λ (1.4) and large λ (1.7), the $h > h_c^+$ states are single phases, FM-M and FM-CO respectively. The FM-CO (for $\lambda/t = 1.7$) eventually gives way to a FM-M beyond $T \sim 0.06$.

We define the λ regime between the red dashed line and green dotted line in Fig.2 as the 'intermediate' λ regime.

In this regime, for (b) and (c) in Fig.4 we find that the $h > h_c^+$ states are inhomogeneous. In the next section we show that the inhomogeneity is due to phase separation (PS) of the system into states of densities different from 0.5. Moreover the constituents vary with changing λ . At

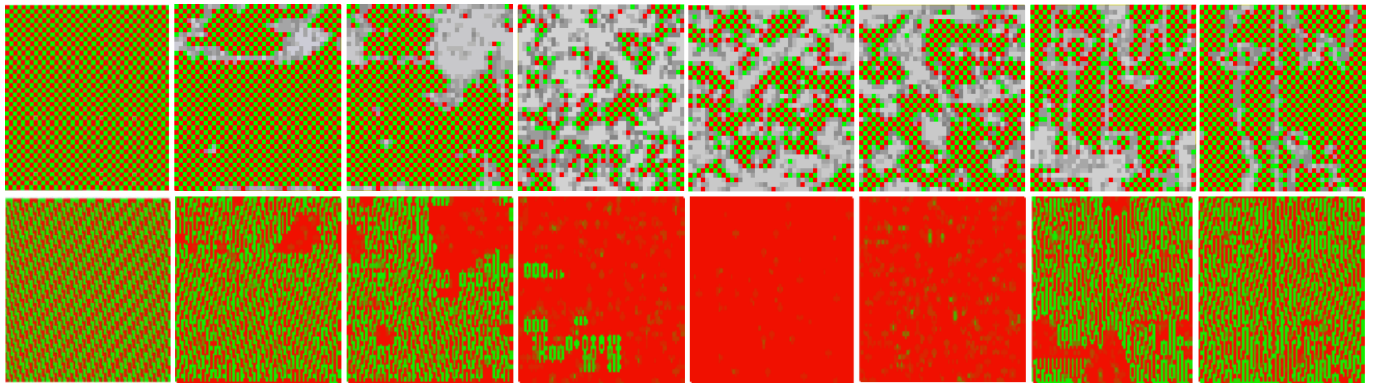


FIG. 5. Colour online: The spatial snapshots of charge ordered region (top panel) at $\lambda/t = 1.55$, $J/t = 0.12$ and the corresponding magnetic bonds (lower panel) at various magnetic fields during a field sweep. Top panel: red-green checker-board are CO regions and gray implies metallic (M) regions. Lower panel, red are FM bonds, green are AF bonds and the zig-zag pattern are CE regions. The field value from left to right are $h/t = 0, 0.05, 0.06, 0.08, 0.20, 0.08, 0.02, 0$. The CE-CO-I state is almost recovered, as seen in the last column, although for perfect recovery very long annealing is required on this 40^2 system.

$\lambda/t \sim 1.5$, the coexisting phases are 'FM-M (n_1) + AF-CD (n_2)' and those at $\lambda/t \sim 1.6$ are 'FM-CO (n_1)+AF-CD(n_2)'.

The evidence of the phase separation (PS) is also seen in Fig.5, where the top panel shows the spatial charge ordering, while the lower panel shows the corresponding magnetic bonds (see figure caption for color convention) for $\lambda/t = 1.55$. These spatial snapshots, at $T/t = 0.02$, are for a 40^2 system and have been obtained from a run in which h is increased from 0 to 0.2 in steps of 0.01, and then reduced to zero in the same sequence. This explicitly shows the inhomogeneous state. However, snapshots based on the Monte Carlo we have employed are likely to be plagued with the system getting stuck in metastable minimas. While we leave the unambiguous determination of PS to the next section, we conclude this one by mentioning what we observe in the snapshots and by raising a question on the true nature of the melting transition, if indeed these snapshots indicate possible PS.

In Fig.5 beginning with the nucleation of FM-M within the CE-CO-I, there occurs a sharp drop in the CO volume fraction in the fourth column and the system breaks up into an inhomogeneous state. In particular we note that at a very large field of $h/t = 0.2$ (fifth column), the composition of the system is FM-M+FM-CO. Reducing the field recovers to zero the CE-CO-I state to a large extent (full recovery requires too large a number of states for such big (40^2) systems, we have checked that on smaller systems we recover the CE-CO-I phase perfectly).

Assuming the above does points towards phase separation tendency beyond h_C^+ raises an important question: Does the equilibrium PS extend only beyond the hysteresis window or does the PS exist at smaller fields as well? If so, how does the hysteresis, between h_C^- and h_C^+ occur on the backdrop of an already equilibrium PS state? We

answer these questions in the next section.

VII. NATURE OF MELTING TRANSITION

Here we deal with two subtle issues, one relates to the existence of equilibrium phase separation and the second is dependence of the field response on sweep rates. The second issue is important because typical sweep experiments are not quasistatic as we infer below and thus it is of interest to understand the interplay of equilibrium phase separation, hysteresis and sweep rates.

A. Equilibrium phase separation

We need to verify that the equilibrium state is indeed phase separated at intermediate fields. This would be distinct from partial trapping of the system in some metastable state. We address this via a fixed μ calculation described below.

We cool the system at different μ , not necessarily targeting half-filling, to explore the vicinity of the $x = 0.50$ state at finite field. This yields the $\mu - n$ characteristic, and the various ground states, at finite h , for a specific choice of electronic parameters. The $\mu - n$ curves are obtained from low temperature μ scans of the system, at fixed h , in a protocol that does not retain the memory of previous μ steps during the μ sweep.

These MC sweeps without memory avoid path dependence, since the system is annealed *ab initio* for each μ , and the fixed μ character allows the system to choose the 'best' possible n , thereby allowing access to the correct phase at any h . Moreover, we ensured that the system has annealed well enough by checking that our results

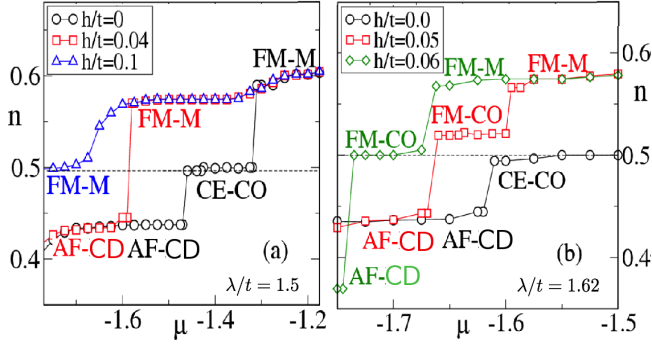


FIG. 6. Colour online: $n - \mu$ curves at $T/t = 0.02$ for $\lambda/t = 1.5$ and $\lambda/t = 1.62$ at indicated magnetic fields. Both cases pass through phase separated states, comprising of (AF-CD and FM-M) for $\lambda/t = 1.5$ and of (AF-CD and FM-CO) for $\lambda/t = 1.62$, before evolving into uniform FM-M in (a) and FM-CO in (b).

hold up to large number (8000) of Monte Carlo steps at each μ . This ensures that the results are well annealed and free from low temperature Monte Carlo problems.

As a numerical check we also allow very long relaxation of the phase separated state within our usual thermal, fixed n , annealing protocol.

As seen in Fig.6(a), for CE-CO-I systems close to the FM-M phase ($\lambda/t \sim 1.5$) the CO is lost beyond $h \sim 0.02$. At a slightly higher field, the system prefers a FM-M state with $n = 0.57$ up to a certain μ and then directly goes to an ‘A-type’ AF phase at $n = 0.44$. If we were to stay at mean density $n = 0.50$ that state would be phase separated, the constituents being the FM-M and the AF-CD phases. This is true for all systems at $\lambda/t \sim 1.45 - 1.6$, and intermediate h . The situation is different for larger coupling, $\lambda/t \sim 1.6 - 1.65$. For a typical case, $\lambda = 1.62$ in Fig.6(b), at intermediate h the system prefers a FM-CO at $n = 0.52$ up to a certain μ and then an AF-CD at $n = 0.44$. Again, if we were to stay at mean density $n = 0.50$ the system will phase separate into the above constituents creating an inhomogeneous state. At larger fields, both in Fig.6(a) and (b), the $n = 0.5$ state becomes stable, recovering the correct asymptotic limits of FM-M for $\lambda/t = 1.5$ and FM-CO for larger $\lambda/t = 1.62$. Apart from confirming the earlier conclusion of inhomogeneous melting, this calculation helps identify the participants in the PS state.

If we now consider the spatial snapshots at large fields ($h/t = 0.20$), fifth column in Fig.5, we find that coexistence of FM-M and FM-CO (for $\lambda/t = 1.55$). However from above, we know that the correct ground state at large fields is FM-M for this range of λ values.

This disagreement is however not unexpected, because at large h (spin polarized limit) the FM-M and FM-CO share a first order boundary and the fixed ‘ n ’ Monte Carlo gets stuck partly in the metastable FM-CO minima. This is the reason we performed the calculations presented in

this section to determine the true equilibrium PS. Similar calculation for $\lambda = 1.4$ and $\lambda = 1.7$ do not yield any phase separation.

B. Sweep dependence

From the $\mu - n$ calculations it is apparent that the melting is inhomogeneous for a range of intermediate e-p couplings. For quasistatic variation of the applied field, for low λ/t (~ 1.4) and high λ/t (> 1.65), the transitions are abrupt. For intermediate λ/t , $\sim 1.45 - 1.65$, the expected transition is continuous. However as we show here, typical experiments, as also the magnetic field sweep rate in our MC, do not allow for enough relaxation making both kinds of transitions appear abrupt.

For this we discuss a schematic of such a transition using the ferromagnetic structure factor as a typical indicator. For intermediate coupling the magnetic phase separation is between an FM and AF states. From their densities one can work out the volume fractions of the two constituent magnetic phases.

Fig.7(a) shows the magnetization with increasing field. The dashed line shows the notional abrupt (first order) transition which is the average of the critical field for transition in the forward and the backward field sweeps. The continuous line depicts the *expected* ‘transition’ whereby the magnetization grows continuously (from CE-type AF state) with increasing h to a FM state. The blue lines are a schematic for the MC response. The hysteresis that is observed occurs in the background of the unusual equilibrium physics involving phase separation. Since the magnetization trace, *i.e.*, the ‘switching’ in hysteresis, depends on the sweep rate let us clarify the experimental and simulation timescales.

The *local* relaxation time τ_{loc} in electronic systems is $\sim 10^{-12}$ seconds, but collective relaxation times τ_{coll} , say, can be macroscopic, ~ 100 seconds in the CO manganites⁹⁴. This experiment was performed at $\sim 0.9T_{CO}$ and τ_{coll} is likely to be much greater at low T . The field cycling periods τ_{per} that we could infer from field melting experiments were⁹⁵ ~ 10 ms. Overall $\tau_{loc} \ll \tau_{per} \ll \tau_{coll}$. Our MC results are broadly in the same window. The ‘microscopic’ timescale is the MC step. The sweep periods were $10^3 - 10^4$ MC steps (bigger in smaller systems) but still $\ll 10^{12}$ that one would need to avoid trapping in a metastable state.

The sweep rate dependence of the switching is illustrated schematically in Fig.7, for an intermediate coupling system. The left panel, (a), is for a quasistatic sweep, $\tau_{per} \gg \tau_{coll}$. In this case there would be only progressive melting and no hysteresis, the system is always in equilibrium. Panel (b) illustrates the regime $\tau_{per} \sim \tau_{coll}$, where the sweep rate is still ‘slow’ but the system cannot quite track the equilibrium state. In this case there could be successive switching. This regime is also out of computational reach for the system sizes we use. Panel (c) is for our regime $\tau_{loc} \ll \tau_{per} \ll \tau_{coll}$. The system

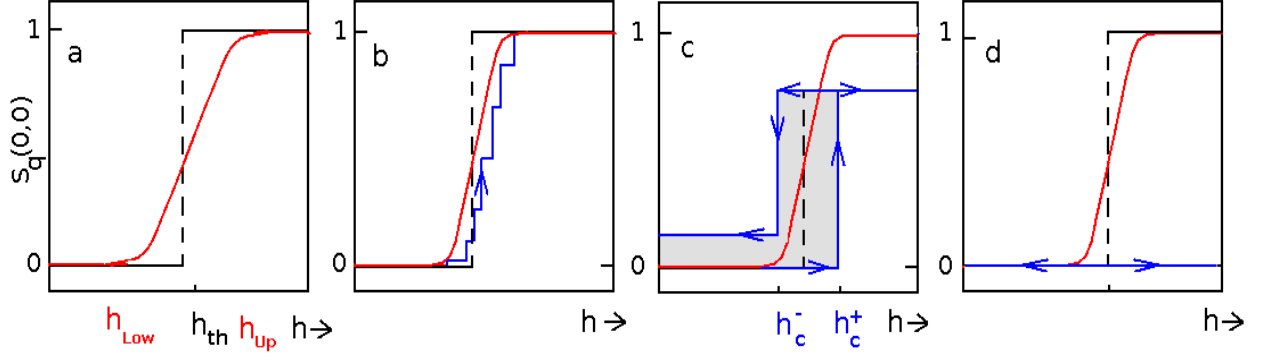


FIG. 7. Schematic sweep rate dependence of the switching at intermediate couplings (λ). (a) Equilibrium evolution of the magnetization, $S_q(0,0)$, with h (red, solid line). h_{th} is a notional value at which a first order transition would have occurred in the absence of PS. The evolution of V_{CO} (blue curves) for different sweep rates is shown in (b)-(d). (b) Slow sweep, (c) fast sweep (our regime, see text), and (d) ultrafast sweep. The text discusses the sweep rates in detail. In (c) the shaded region depicts hysteresis.

switches at h_c^+ on field increase, but not necessarily to the underlying equilibrium state. The magnetization, V_{CO} , etc, are determined by the presence of metastable states. For $h \gg h_c^+$, where the equilibrium state is a homogeneous FM (at this λ) the low temperature system can still remain trapped in the metastable state. We expect similar reasons to cause non-recovery in the backward sweep when the λ and J/t are such that the FM-M is still metastable when the system is swept back. Finally, (d) is for an ultrafast sweep, $\tau_{per} \sim \tau_{loc}$, where the system is unable to respond at all to the changing field.

As shown in panel (c), for sweep rates typical in the experiments and in our calculation, the high field state is influenced by the equilibrium PS and nearby metastable states. This can be seen in the field sweep spatial snapshots of Fig.5 for $\lambda/t = 1.55$. At $h/t = 0.08$ (column four), we find that the state arises from a combination of equilibrium AF-M + FM-M phase coexistence and a metastable FM-CO. Increasing h/t to 0.2 (column 5) converts the AF-M to FM-M but the metastable FM-CO fraction can be removed only by thermal annealing.

VIII. LANDAU FRAMEWORK FOR FIELD MELTING

Over the earlier sections, we drew a number of conclusions regarding the λ dependence of the magnetic response. Here we suggest a Landau free energy landscape involving the relevant competing phases and organize the field response within a single framework.

While we do not present a Landau functional here, based on our results we schematically show an energy landscape in terms of some generalized order parameter. While deriving such a theory from the microscopic model is difficult, a heuristic construction could still be useful as an organizing tool. A Landau theory with the provision of stabilizing both commensurate CO at half doping and incommensurate order off half doping⁹⁶ and the con-

comitant magnetic order has been studied before. This reproduces the qualitative $x - T$ phase diagram around half doping and exhibits phase coexistence in absence of either strain or disorder. Our landscape can help improve such constructs.

From the previous sections we know that the melting can either be homogeneous or inhomogeneous. For $\lambda/t < 1.6$ the system can melt the CO simply by lowering the energy of the FM-M minimum with increase in h . The increase in field can either lead to a simple first order transition, as happens for $\lambda/t \sim 1.40$ or lead to PS as happens for intermediate λ . In either case the loss of CO volume fraction is guaranteed. However for $\lambda/t \sim 1.6 - 1.65$, the FM-CO is closest in energy to the CE-CO-I (and also the true ground state in the limit of $h \rightarrow \infty$). Without the intermediate h phase separation, the CE-CO-I would have simply gone over to the FM-CO phase, as happens for $\lambda/t > 1.65$. *The phase separation is necessary for the destabilization of the CO for this λ window.*

With this general understanding, let us discuss the Landau landscape shown in Fig.8. This has three panels depicting the free energy landscapes with increasing magnetic fields for three increasing values of λ .

Small λ response: Panel (a) of Fig.8 corresponds to $\lambda/t \sim 1.5$, where the CO state melts beyond a critical field but does not recover when the field is swept back. The $h = 0$ landscape has CE-CO-I as the global minimum and the FM-M is metastable. This metastable FM-M is responsible for the non recovery of the CE-CO-I state when h is swept back to zero. From $h = h_1$ to h_2 , the FM-M minimum lowers as expected with increasing field. If the λ/t is small, ~ 1.4 , this continues leading to a first order transition to a homogeneous FM-M. However, if $\lambda/t \sim 1.5$, at h_2 the system phase separates into off half doping phase (AF-CD + FM-M), these two minima are depicted in panel (a). On further increasing the field the system evolves into the large field $n = 0.50$ FM-M ground state. The phase that is closest in energy to this is the

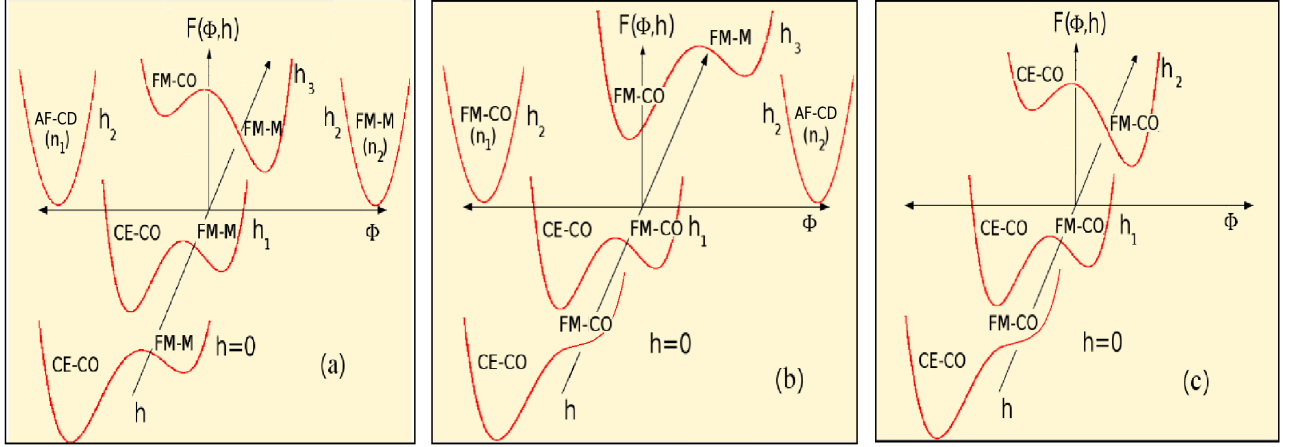


FIG. 8. Colour online: The low temperature Landau free energy landscape with the magnetic field axis going into the plane of the paper and the other axis, Φ , being the general order parameter axis. The three panels (a), (b) and (c) are representative of $\lambda/t = 1.5$, $\lambda/t = 1.6$ and $\lambda/t > 1.65$ respectively. All the phases are at electron density $n = 0.5$, except the ones for which a density are shown in brackets along with the name of the phase. The intervening A-type AF region is not shown to avoid cluttering.

FM-CO, as is seen in Fig.2 at low J/t and $\lambda/t \sim 1.5$. Given the tendency to get trapped in the FM-CO, we depict this state as metastable at large fields.

Intermediate λ response: Panel.(b) shows a similar landscape for $\lambda/t \sim 1.60 - 1.65$. There are a few important differences compared to panel.(a). (i) From Fig.2 the FM-CO phase is the closest to the CE-CO-I phase, that can be accessed by a magnetic field. (ii) Since we know that the CE-CO phase is recovered when the field is swept back, in the $h = 0$ landscape the FM-CO has to be unstable, as opposed to the FM-M being metastable at $h = 0$ in (a). (iii) The phase separation at intermediate fields is between FM-CO and AF-CD as depicted, which are off half doping phases. (iv) Finally, at large h the FM-CO is the global minimum and the FM-M minima is metastable, as is seen Fig.2 at low J .

Large λ response: This is shown in panel.(c). Like the small λ systems, the large λ systems have a simple field evolution. As in (b), the phase closest in energy to the CE-CO is the FM-CO and since the CE-CO state is recovered when the field is swept back to zero, this FM-CO state should be unstable at $h = 0$. With increasing h the FM-CO energy would lower and finally replacing the CE-CO as the global minimum. At large fields (not shown) the CE-CO would become unstable. Note here the CO does not melt and, in this view, if the intermediate h PS did not occur for $\lambda/t \sim 1.60 - 1.65$, CO melting would not have been possible. This we believe is an important observation.

IX. CONCLUSIONS

We reported the first controlled results on the field melting of charge order in half doped manganites using an

unbiased Monte Carlo method. We showed how magnetic field sweep rate induced non-equilibrium physics plays out on the background of equilibrium phase separation, governing the response to magnetic fields and creating inhomogeneous phases without disorder. Our framework to incorporate field melting response within a free energy landscape can aid construction of Landau theories for these materials.

Recent experiments^{97,98} have followed up older work⁹⁹⁻¹⁰¹ on features seen in the magnetization curve with magnetic field sweep. These results are close to half doping or with small doping of the Mn site. The most recent experiment⁹⁷ finds step like features for slow sweep rate (1T/s), which gives way to an abrupt transition with two metamagnetic anomalies for large sweep rates (10³T/s). These are consistent with our conclusions discussed in Sec. VII, however the true equilibrium continuous transition can be mapped only for much smaller sweep rates. We hope such experiments would be performed in future. More generally, these results bring out the importance of relaxation of correlated degrees of freedom in understanding current experiments employing time dependent external probes on such materials.

We acknowledge use of the Beowulf cluster at HRI. PM was supported by a DAE-SRC Outstanding Research Investigator grant, and the DST India.

- ¹ R. von Helmolt, J. Wecker, B. Holzapfel, L. Schultz, and K. Samwer, *Phys. Rev. Lett.* **71**, 2331 (1993).
- ² S. Jin, T. H. Tiefel, M. McCormack, R. A. Fastnacht, R. Ramesh, and L. H. Chen, *Science* **264**, 413 (1994).
- ³ T. Kimura, T. Goto, H. Shintani, K. Ishizaka, T. Arima, and Y. Tokura, *Nature* **426**, 55 (2003).
- ⁴ See, *Colossal Magnetoresistive Oxides*, edited by Y. Tokura, Gordon and Breach, Amsterdam (2000).
- ⁵ T. Hotta and E. Dagotto, In *Colossal Magnetoresistive Manganites*, edited by T. Chatterji, Kluwer Academic Publishers, Dordrecht, Netherlands (2002).
- ⁶ J. Zhang and R. Averitt, *Annual Review of Materials Research* **44**, 19 (2014), cited By (since 1996)0.
- ⁷ D. Basov, R. Averitt, D. Van Der Marel, M. Dressel, and K. Haule, *Reviews of Modern Physics* **83**, 471 (2011).
- ⁸ Y. Tokura, *Reports on Progress in Physics* **69**, 797 (2006).
- ⁹ D. Okuyama, M. Nakamura, Y. Wakabayashi, H. Itoh, R. Kumai, H. Yamada, Y. Taguchi, T. Arima, M. Kawasaki, and Y. Tokura, *Applied Physics Letters* **95**, 152502 (2009).
- ¹⁰ J. Wang, F. X. Hu, R. W. Li, J. R. Sun, and B. G. Shen, *Applied Physics Letters* **96**, 052501 (2010).
- ¹¹ G. Wang, D. Chen, D. Wu, and A. Li, *Physica B: Condensed Matter* **434**, 106 (2014).
- ¹² M. Garganourakis, V. Scagnoli, S. W. Huang, U. Staub, H. Wadati, M. Nakamura, V. A. Guzenko, M. Kawasaki, and Y. Tokura, *Phys. Rev. Lett.* **109**, 157203 (2012).
- ¹³ H. Boschker, J. Kautz, E. P. Houwman, W. Siemons, D. H. A. Blank, M. Huijben, G. Koster, A. Vailionis, and G. Rijnders, *Phys. Rev. Lett.* **109**, 157207 (2012).
- ¹⁴ T. Z. Ward, J. D. Budai, Z. Gai, J. Z. Tischler, L. Yin, and J. Shen, *Nature Physics* **5**, 885 (2009).
- ¹⁵ E. J. Monkman, C. Adamo, J. A. Mundy, D. E. Shai, J. W. Harter, D. Shen, B. Burganov, D. A. Muller, D. G. Schlom, and K. M. Shen, *Nature Materials* **11**, 855 (2012).
- ¹⁶ S. J. May, P. J. Ryan, J. L. Robertson, J. W. Kim, T. S. Santos, E. Karapetrova, J. L. Zarestky, X. Zhai, S. G. E. te Velthuis, J. N. Eckstein, S. D. Bader, and A. Bhatlacharya, *Nature Materials* **8**, 892 (2009).
- ¹⁷ H. Y. Hwang, Y. Iwasa, M. Kawasaki, B. Keimer, N. Nagasawa, and Y. Tokura, *Nature Materials* **11**, 103 (2012).
- ¹⁸ M. Gibert, *Nature Materials* **11**, 195 (2012).
- ¹⁹ H. Jeon and A. Biswas, *Phys. Rev. B* **88**, 024415 (2013).
- ²⁰ A. Rebello and R. Mahendiran, *Applied Physics Letters* **96**, 152504 (2010).
- ²¹ T. Hatano, Y. Ogimoto, N. Ogawa, M. Nakano, S. Ono, Y. Tomioka, K. Miyano, Y. Iwasa, and Y. Tokura, *Scientific Reports* **3**, 2904 (2013).
- ²² I. Pallecchi, L. Pellegrino, E. Bellingeri, A. S. Siri, and D. Marre, *Journal of Applied Physics* **95**, 8079 (2004).
- ²³ S. M. Wu, S. A. Cybart, P. Yu, M. D. Rossell, J. X. Zhang, R. Ramesh, and R. C. Dynes, *Nature Materials* **9**, 756 (2010).
- ²⁴ Z. G. Sheng, M. Nakamura, W. Koshibae, T. Makino, Y. Tokura, and M. Kawasaki, *Nature Communications* **5**, 4584 (2014).
- ²⁵ A. J. Millis, P. B. Littlewood, and B. I. Shraiman, *Phys. Rev. Lett.* **74**, 5144 (1995).
- ²⁶ E. Dagotto, T. Hotta, and A. Moreo, *Physics Reports* **344**, 1 (2001).
- ²⁷ M. Rini, R. Tobey, N. Dean, J. Itatani, Y. Tomioka, Y. Tokura, R. W. Schoenlein, and A. Cavalleri, *Nature* **449**, 72 (2007).
- ²⁸ Y. Li, D. Walko, Q. Li, Y. Liu, S. Rosenkranz, H. Zheng, J. Mitchell, H. Wen, E. Dufresne, and B. Adams, *Materials Research Society Symposium Proceedings* **1636** (2014).
- ²⁹ A. Caviezel, U. Staub, S. Johnson, S. Mariager, E. Mhr-Vorobeva, G. Ingold, C. Milne, M. Garganourakis, V. Scagnoli, S. Huang, Q. Jia, S.-W. Cheong, and P. Beaud, *Phys. Rev. B* **86** (2012).
- ³⁰ D. Polli, M. Rini, S. Wall, R. W. Schoenlien, Y. Tomioka, Y. Tokura, G. Cerullo, and A. Cavalleri, *Nature Materials* **6**, 643 (2007).
- ³¹ H. Matsuzaki, H. Uemura, M. Matsubara, T. Kimura, Y. Tokura, and H. Okamoto, *Phys. Rev. B* **80**, 115128 (2009).
- ³² H. Kuwahara, Y. Tomioka, A. Asamitsu, Y. Moritomo, and Y. Tokura, *Science* **270**, 961 (1995).
- ³³ Y. Tomioka, A. Asamitsu, Y. Moritomo, H. Kuwahara, and Y. Tokura, *Phys. Rev. Lett.* **74**, 5108 (1995).
- ³⁴ W. Wu, C. Israel, N. Hur, S. Park, S.-W. Cheong, and A. de Lozanne, *Nature Materials* **5**, 881 (2006).
- ³⁵ M. Quintero, J. Sacanell, L. Ghivelder, A. M. Gomes, A. G. Leyva, and F. Parisi, *Applied Physics Letters* **97**, 121916 (2010).
- ³⁶ M. Quintero, F. Parisi, G. Leyva, and L. Ghivelder, *Journal of Physics: Condensed Matter* **20**, 345204 (2008).
- ³⁷ J. Sacanell, F. Parisi, P. Levy, and L. Ghivelder, *Physica B: Condensed Matter* **354**, 43 (2004), proceedings of the Workshop "At the Frontiers of Condensed Matter". Magnetism, Magnetic Materials, and their Applications.
- ³⁸ J. Sacanell, M. Quintero, J. Curiale, G. Garbarino, C. Acha, R. S. Freitas, L. Ghivelder, G. Polla, G. Leyva, P. Levy, and F. Parisi, *Journal of Alloys and Compounds* **369**, 74 (2004), proceedings of the {VI} Latin American Workshop on Magnetism, Magnetic Materials and their Applications.
- ³⁹ M. Respaud, A. Llobet, C. Frontera, C. Ritter, J. M. Broto, H. Rakoto, M. Goiran, and J. L. Garcia-Munoz, *Phys. Rev. B* **61**, 9014 (2000).
- ⁴⁰ Y. Tokura, H. Kuwahara, Y. Moritomo, Y. Tomioka, and A. Asamitsu, *Phys. Rev. Lett.* **76**, 3184 (1996).
- ⁴¹ H. Kawano, R. Kajimoto, H. Yoshizawa, Y. Tomioka, H. Kuwahara, and Y. Tokura, *Phys. Rev. Lett.* **78**, 4253 (1997).
- ⁴² H. Kuwahara, Y. Moritomo, Y. Tomioka, A. Asamitsu, M. Kasai, R. Kumai, and Y. Tokura, *Phys. Rev. B* **56**, 9386 (1997).
- ⁴³ A. Kirste, M. Goiran, M. Respaud, J. Vanaken, J. M. Broto, H. Rakoto, M. von Ortenberg, C. Frontera, and J. L. Garcia-Munoz, *Phys. Rev. B* **67**, 134413 (2003).
- ⁴⁴ A. Trokiner, S. Verkhovskii, A. Yakubovskii, K. Kumagai, P. Monod, K. Mikhalev, A. Buzlukov, Y. Furukawa, N. Hur, and S.-W. Cheong, *Phys. Rev. B* **77**, 134436 (2008).
- ⁴⁵ C. H. Chen, S. Mori, and S.-W. Cheong, *Phys. Rev. Lett.* **83**, 4792 (1999).
- ⁴⁶ C. H. Chen and S.-W. Cheong, *Phys. Rev. Lett.* **76**, 4042 (1996).
- ⁴⁷ P. Chaddah, K. Kumar, and A. Banerjee, *Phys. Rev. B*

- 77**, 100402 (2008).
- ⁴⁸ K. Kumar, A. K. Pramanik, A. Banerjee, P. Chaddah, S. B. Roy, S. Park, C. L. Zhang, and S.-W. Cheong, *Phys. Rev. B* **73**, 184435 (2006).
 - ⁴⁹ S. K. Mishra, R. Pandit, and S. Satpathy, *Phys. Rev. B* **56**, 2316 (1997).
 - ⁵⁰ S. Fratini, D. Feinberg, and M. Grilli, *The European Physical Journal B - Condensed Matter and Complex Systems* **22**, 157 (2001).
 - ⁵¹ O. Cépas, H. R. Krishnamurthy, and T. V. Ramakrishnan, *Phys. Rev. B* **73**, 035218 (2006).
 - ⁵² T. Hotta, A. L. Malvezzi, and E. Dagotto, *Phys. Rev. B* **62**, 9432 (2000).
 - ⁵³ A. Mukherjee and P. Majumdar, *The Eur. Phys. J B* **87**, 239 (2014).
 - ⁵⁴ A. Mukherjee, K. Pradhan, and P. Majumdar, *EPL (Europhysics Letters)* **86**, 27003 (2009).
 - ⁵⁵ L. M. Rodriguez-Martinez and J. P. Attfield, *Phys. Rev. B* **63**, 024424 (2000).
 - ⁵⁶ L. M. Rodriguez-Martinez and J. P. Attfield, *Phys. Rev. B* **54**, R15622 (1996).
 - ⁵⁷ Y. Tomioka and Y. Tokura, *Phys. Rev. B* **70**, 014432 (2004).
 - ⁵⁸ D. Akahoshi, M. Uchida, Y. Tomioka, T. Arima, Y. Matsui, and Y. Tokura, *Phys. Rev. Lett.* **90**, 177203 (2003).
 - ⁵⁹ H. Das, G. Sangiovanni, A. Valli, K. Held, and T. Saha-Dasgupta, *Phys. Rev. Lett.* **107**, 197202 (2011).
 - ⁶⁰ C. Şen, S. Liang, and E. Dagotto, *Phys. Rev. B* **85**, 174418 (2012).
 - ⁶¹ S. Kumar, A. P. Kampf, and P. Majumdar, *Phys. Rev. Lett.* **97**, 176403 (2006).
 - ⁶² J. van den Brink, G. Khaliullin, and D. Khomskii, *Phys. Rev. Lett.* **83**, 5118 (1999).
 - ⁶³ S. Kumar, J. van den Brink, and A. P. Kampf, *Phys. Rev. Lett.* **104**, 017201 (2010).
 - ⁶⁴ L. Brey, *Phys. Rev. Lett.* **92**, 127202 (2004).
 - ⁶⁵ L. Brey and P. B. Littlewood, *Phys. Rev. Lett.* **95**, 117205 (2005).
 - ⁶⁶ D. V. Efremov, J. van den Brink, and D. I. Khomskii, *Nature Materials* **3**, 853 (2004).
 - ⁶⁷ P. Barone, S. Picozzi, and J. van den Brink, *Phys. Rev. B* **83**, 233103 (2011).
 - ⁶⁸ S. Kumar and P. Majumdar, *Phys. Rev. Lett.* **96**, 016602 (2006).
 - ⁶⁹ S. Kumar, A. P. Kampf, and P. Majumdar, *Phys. Rev. B* **75**, 014209 (2007).
 - ⁷⁰ K. Pradhan, A. Mukherjee, and P. Majumdar, *Phys. Rev. Lett.* **99**, 147206 (2007).
 - ⁷¹ J. van den Brink, P. Horsch, F. Mack, and A. M. Oleś, *Phys. Rev. B* **59**, 6795 (1999).
 - ⁷² J. Salafranca, R. Yu, and E. Dagotto, *Phys. Rev. B* **81**, 245122 (2010).
 - ⁷³ S. Kumar and P. Majumdar, *Phys. Rev. Lett.* **94**, 136601 (2005).
 - ⁷⁴ C. Şen, G. Alvarez, and E. Dagotto, *Phys. Rev. Lett.* **105**, 097203 (2010).
 - ⁷⁵ C. Şen, G. Alvarez, and E. Dagotto, *Phys. Rev. Lett.* **98**, 127202 (2007).
 - ⁷⁶ C. Şen, G. Alvarez, Y. Motome, N. Furukawa, I. A. Sergienko, T. C. Schulthess, A. Moreo, and E. Dagotto, *Phys. Rev. B* **73**, 224430 (2006).
 - ⁷⁷ S. Dong and E. Dagotto, *Phys. Rev. B* **87**, 195116 (2013).
 - ⁷⁸ S. Dong, Q. Zhang, S. Yunoki, J.-M. Liu, and E. Dagotto, *Phys. Rev. B* **86**, 205121 (2012).
 - ⁷⁹ A. Baena, L. Brey, and M. J. Calderón, *Phys. Rev. B* **83**, 064424 (2011).
 - ⁸⁰ A. Mukherjee, W. S. Cole, P. Woodward, M. Randeria, and N. Trivedi, *Phys. Rev. Lett.* **110**, 157201 (2013).
 - ⁸¹ I. A. Sergienko, C. Şen, and E. Dagotto, *Phys. Rev. Lett.* **97**, 227204 (2006).
 - ⁸² M. J. Calderón, S. Liang, R. Yu, J. Salafranca, S. Dong, S. Yunoki, L. Brey, A. Moreo, and E. Dagotto, *Phys. Rev. B* **84**, 024422 (2011).
 - ⁸³ S. Dong and E. Dagotto, *Phys. Rev. B* **88**, 140404 (2013).
 - ⁸⁴ G. Giovannetti, S. Kumar, D. Khomskii, S. Picozzi, and J. van den Brink, *Phys. Rev. Lett.* **103**, 156401 (2009).
 - ⁸⁵ G. Giovannetti, S. Kumar, J. van den Brink, and S. Picozzi, *Phys. Rev. Lett.* **103**, 037601 (2009).
 - ⁸⁶ G. Giovannetti, S. Kumar, C. Ortix, M. Capone, and J. van den Brink, *Phys. Rev. Lett.* **109**, 107601 (2012).
 - ⁸⁷ S. Kumar and P. Majumdar, *The European Physical Journal B - Condensed Matter and Complex Systems* **50**, 571 (2006).
 - ⁸⁸ B. L. Li, X. P. Liu, F. Fang, J. L. Zhu, and J.-M. Liu, *Phys. Rev. B* **73**, 014107 (2006).
 - ⁸⁹ M. Rao, H. R. Krishnamurthy, and R. Pandit, *Phys. Rev. B* **42**, 856 (1990).
 - ⁹⁰ K. Binder and D. P. Landau, *Phys. Rev. B* **30**, 1477 (1984).
 - ⁹¹ D. P. Landau and K. Binder, *Phys. Rev. B* **17**, 2328 (1978).
 - ⁹² S. Kumar and P. Majumdar, *The European Physical Journal B - Condensed Matter and Complex Systems* **46**, 237 (2005).
 - ⁹³ K. Pradhan, A. Mukherjee, and P. Majumdar, *Phys. Rev. Lett.* **99**, 147206 (2007).
 - ⁹⁴ J. Sacanell, F. Parisi, P. Levy, and L. Ghivelder, *Physica B: Condensed Matter* **354**, 43 (2004), proceedings of the Workshop.
 - ⁹⁵ M. Tokunaga, N. Miura, Y. Tomioka, and Y. Tokura, *Phys. Rev. B* **60**, 6219 (1999).
 - ⁹⁶ G. C. Milward, M. J. Calderón, and P. B. Littlewood, *Nature* **433**, 607 (2005).
 - ⁹⁷ Z. W. Ouyang, H. Nojiri, and S. Yoshii, *Phys. Rev. B* **78**, 104404 (2008).
 - ⁹⁸ A. V. Kalinov, L. M. Fisher, I. F. Voloshin, N. A. Babushkina, C. Martin, and A. Maignan, *Journal of Physics: Conference Series* **150**, 042081 (2009).
 - ⁹⁹ S. Hbert, A. Maignan, V. Hardy, C. Martin, M. Hervieu, and B. Raveau, *Solid State Communications* **122**, 335 (2002).
 - ¹⁰⁰ V. Hardy, S. Hbert, A. Maignan, C. Martin, M. Hervieu, and B. Raveau, *Journal of Magnetism and Magnetic Materials* **264**, 183 (2003).
 - ¹⁰¹ T. Wu and J. Mitchell, *Journal of Magnetism and Magnetic Materials* **292**, 25 (2005).